Check for updates

Geophysical Research Letters

RESEARCH LETTER
10.1029/2023GL104697

Key Points:

- Satellite data show long-term Bering Strait flow increase may be due to increasing westward winds in the summer Arctic and fall Bering Sea
- Data imply large (0.17 psu/year) East Siberian Sea salinization, likely due to hitherto unappreciated increasing Pacific inflow to that region
- Use of older Ocean Bottom Pressure data or poor salinity representation may explain failure of models to simulate observed flow increase

Supporting Information:

Supporting Information may be found in the online version of this article.

Correspondence to:

C. Peralta-Ferriz,
ferriz@uw.edu

Citation:

Peralta-Ferriz, C., & Woodgate, R. A. (2023). Arctic and sub-Arctic mechanisms explaining observed increasing northward flow through the Bering Strait and why models may be getting it wrong. *Geophysical Research Letters*, *50*, e2023GL104697. https://doi.org/10.1029/2023GL104697

Received 31 MAY 2023
Accepted 30 NOV 2023

Author Contributions:

Conceptualization: Cecilia Peralta-Ferriz, Rebecca A. Woodgate
Data curation: Cecilia Peralta-Ferriz, Rebecca A. Woodgate
Formal analysis: Cecilia Peralta-Ferriz, Rebecca A. Woodgate
Funding acquisition: Cecilia Peralta-Ferriz, Rebecca A. Woodgate
Investigation: Cecilia Peralta-Ferriz, Rebecca A. Woodgate
Methodology: Cecilia Peralta-Ferriz, Rebecca A. Woodgate

© 2023. The Authors.
This is an open access article under the terms of the Creative Commons Attribution-NonCommercial-NoDerivs License, which permits use and distribution in any medium, provided the original work is properly cited, the use is non-commercial and no modifications or adaptations are made.

Arctic and Sub-Arctic Mechanisms Explaining Observed Increasing Northward Flow Through the Bering Strait and Why Models May Be Getting It Wrong

Cecilia Peralta-Ferriz[1] **and Rebecca A. Woodgate**[1]

[1]University of Washington, Seattle, WA, USA

Abstract The Pacific oceanic input to the Arctic via the Bering Strait (important for western Arctic ice retreat, water properties, and nutrient supply) has been increasing for three decades. Using satellite Ocean Bottom Pressure (OBP) and Dynamic Ocean Topography (DOT) data, we show that long-term trends in mooring data for a well-sampled sub-period (2003–2014) relate to summer OBP and DOT drop in the Arctic's East Siberian Sea (ESS), in turn caused by stronger westward ESS winds, and increased fall westward winds in the Bering Sea. OBP/DOT differences imply strong (0.17 psu/year) ESS salinization, likely caused by hitherto unappreciated increased Pacific inflow to that region. We find ESS OBP trends are (erroneously) reversed in older data versions, and estimate that ESS salinization may significantly mediate Bering Strait flow increase. These facts may explain why models assimilating older OBP data, or with erroneous Bering Strait salinities, fail to simulate observed Bering Strait flow increase.

Plain Language Summary Direct year-round, in-water measurements show the Pacific oceanic flow to the Arctic (which is only via the narrow Bering Strait) has been increasing for three decades. This flow is important to the region as it triggers seasonal ice retreat in the Pacific side of the Arctic, the "western Arctic," and strongly influences the temperature, salinity, and nutrient content of western Arctic waters. Using satellite data sets that measure the height of the sea surface, and how it changes, we find we can explain the 2003–2014 observed flow increase by increased westward winds in the Arctic in summer and in the Bering Sea in fall. These satellite data sets also imply parts of the coastal western Arctic have become much saltier over this period, likely due to previously unsuspected increased Pacific input to the region. This increased salinity acts to slow the increasing flow to the Arctic. We find older versions of some of these satellite data sets are inconsistent with the observed flow increase. Most model simulations of the Arctic do not currently capture the observed flow increase. We suggest this may be due to fitting these models to older (erroneous) satellite data sets, or having poor representation of the salinity of Pacific waters.

1. Introduction

The oceanic Pacific inflow to the Arctic via the Bering Strait dominates the water properties of the Chukchi Sea, triggers Chukchi and western Arctic sea-ice retreat, and provides nutrients, freshwater, and heat to the western Arctic and beyond (e.g., Woodgate, 2018). Year-round in situ Bering Strait moorings (1990-present, Woodgate, 2018) show strong seasonal and interannual variability and significant long-term warming, freshening, and flow increase (1991–2021: 0.03 ± 0.02°C/year; 0.010 ± 0.007 psu/year, and 0.010 ± 0.005 Sv/year, i.e., 0.23 ± 0.12 cm/s/year), which in combination drive large increases in heat and freshwater fluxes to the Arctic (1991–2021: $6.4 \pm 3.7 \times 10^{18}$ J/year relative to −1.9°C and 33 ± 15 km^3/year relative to 34.8 psu), with flow strengthening being a major driver of heat and freshwater flux changes (trends updated from Woodgate & Peralta-Ferriz, 2021). However, the causes of this long-term flow increase are unknown. Indeed, most numerical simulations show either no-trend, or a decreasing trend (e.g., Jahn & Laiho, 2020; Nguyen et al., 2020), contradicting observational evidence.

Prior work (Woodgate et al., 2005) has typically separated the Bering Strait flow into locally and far-field forced components. Northward velocity (from mooring data) is well correlated ($r \sim 0.8$) with the almost northward (heading ~330°) local wind, explainable by geostrophic balance to a wind-driven across-strait pressure-gradient set-up (Woodgate, 2018). However, not all the flow variance matches local wind variability and flow is northward when local winds are zero. These facts are attributed to a far-field, Pacific-Arctic "pressure-head" (PH), forcing, which has never been directly observed, but only inferred, and it is unclear between which points this pressure

Project Administration: Cecilia Peralta-Ferriz, Rebecca A. Woodgate
Resources: Cecilia Peralta-Ferriz, Rebecca A. Woodgate
Supervision: Cecilia Peralta-Ferriz, Rebecca A. Woodgate
Validation: Cecilia Peralta-Ferriz, Rebecca A. Woodgate
Visualization: Cecilia Peralta-Ferriz, Rebecca A. Woodgate
Writing – original draft: Cecilia Peralta-Ferriz, Rebecca A. Woodgate
Writing – review & editing: Cecilia Peralta-Ferriz, Rebecca A. Woodgate

gradient might be measured. Originally assumed to be constant (Coachman & Aagaard, 1966), this PH term is generally attributed to Pacific sea-level being higher than Arctic sea-level, due to either the global freshwater balance (Stigebrandt, 1984) or global winds (De Boer and Nof, 2004a, 2004b). Long time-series, however, show the PH term to be time-variable (Woodgate et al., 2005), and studies assign its variability to Arctic/sub-Arctic winds or shelf waves (Danielson et al., 2014; Nguyen et al., 2020; Peralta-Ferriz & Woodgate, 2017). Note that observations indicate that the long-term flow increase is due to increase in the PH term (Woodgate & Peralta-Ferriz, 2021).

In a particular breakthrough, Peralta-Ferriz and Woodgate (2017), using satellite Ocean Bottom Pressure (OBP) data from the Gravity Recovery and Climate Experiment (GRACE) mission (Tapley et al., 2004, 2019), found a strong correlation between the PH term and the time-variability of the first Empirical Orthogonal Function (EOF) of OBP in the Bering/Chukchi region, that is, from the northern Bering Sea to the western Arctic ($r = 0.6$ year-round, $r = 0.84$ in June–July–August [JJA] season). The EOF pattern—low in the Arctic's East Siberian Sea (ESS), high over the Bering Sea Shelf southeast of the strait—matches the sea surface height/bottom pressure pattern of geostrophic flow through a rotating channel (Toulany & Garrett, 1984), implying that low OBP in the ESS (e.g., from Ekman off-shelf transport driven by westward Arctic shelf-break winds) draws water northward through the strait. This mechanism shares features with Danielson et al. (2014)'s Bering Sea/ESS wind-driven hypothesis, although they attribute ∼90% of the variance to Bering Sea forcings. We propose now that this mechanism, proven for monthly variability, may also explain part of the long-term trend.

Using theory (Section 3) and satellite and in situ data sets (Section 4), we quantify trends in the Arctic and sub-Arctic drivers of the flow. Our work also suggests that the remarkable salinization of the ESS implied by these data is explainable by increased Pacific inflow (Section 5), uncovers disturbing consequences of using older versions of GRACE products, and offers insights into why models may be missing the observed Bering Strait flow increase (Sections 6 and 7).

2. Data, and Time Period of the Study

We use the satellite data sets of (a) GRACE JPL Mascons (primarily Release 6 version 2, but also earlier versions) global OBP (Watkins et al., 2015; Wiese et al., 2016, 2018), available monthly from 2002 to 2017, gridded at 0.5° × 0.5° resolution (effective resolution from satellite footprint ∼300 km), and (b) Envisat and CryoSat Dynamic Ocean Topography (DOT) data (Armitage et al., 2016), available monthly from 2003 to 2014 for 60°N to 81.5°N, and gridded at 0.75° × longitude × 0.25° latitude. Uncertainties are estimated as 1.1 cm for DOT, and between 1 and 2 cm for OBP. The GRACE data used are an updated version of those used by Peralta-Ferriz and Woodgate (2017), but show essentially the same correlation/EOF analysis for the month-to-month variability analysis.

We restrict our analysis to the period of this original DOT data (2003–2014) to avoid spurious long-term trends that may arise when extending time-series by combining different satellites or analysis methods.

Monthly-mean surface wind velocity, wind stress, and sea-level pressure data are taken from the NCEP-NCAR Reanalysis 1 (Kalnay et al., 1996) (the reanalysis best matching Bering Strait wind observations, Woodgate, 2018), provided on a global 2.5° × 2.5° grid. NCEP wind stresses are defined as stress on the atmosphere. We estimate the surface stress on the ocean (henceforth "ocean surface stress") as the negative of the NCEP wind stress, recognizing this neglects momentum lost to sea-ice processes.

As in Peralta-Ferriz and Woodgate (2017), we use monthly estimates of the Bering Strait total northward flow (VVEL) and PH term, calculated from the in situ data of the midstrait "climate site" mooring (A3). The PH term is the residual of a monthly fit of 6-hrly NCEP wind (Kalnay et al., 1996) to the total flow (see Woodgate, 2018). Monthly sea-ice concentrations, spatial resolution of 25 × 25 km, are from NOAA/NSIDC Passive Microwave Version 3 (Meier et al., 2017; Peng et al., 2013).

Sea surface temperature (SST) data are from the version 4.1 Multiscale Ultrahigh Resolution (MUR) Level-4 analysis product (Chin et al., 2017; JPL MUR MEaSUREs Project, 2015), provided on a daily global 0.01° × 0.01° resolution grid.

Trends, correlations, and regressions are calculated from monthly values (for consistency across data sets) and are only shown when significant at the 95% level (unless indicated otherwise), using an integral timescale to estimate degrees of freedom (Woodgate, 2018).

19448007, 2023, 24, Downloaded from https://agupubs.onlinelibrary.wiley.com/doi/10.1029/2023GL104697 by Test, Wiley Online Library on [01/01/2024]. See the Terms and Conditions (https://onlinelibrary.wiley.com/terms-and-conditions) on Wiley Online Library for rules of use; OA articles are governed by the applicable Creative Commons License

19448007, 2023, 24, Downloaded from https://agupubs.onlinelibrary.wiley.com/doi/10.1029/2023GL104697 by Test, Wiley Online Library on [01/01/2024]. See the Terms and Conditions (https://onlinelibrary.wiley.com/terms-and-conditions) on Wiley Online Library for rules of use; OA articles are governed by the applicable Creative Commons License

3. Theory and Observations of Drivers of the Bering Strait Throughflow

Since GRACE data employs some trend corrections in time (e.g., Watkins et al., 2015), to ensure robustness of our conclusions, we first expand our prior GRACE work (Peralta-Ferriz & Woodgate, 2017) to include the independent data set of DOT—a measure of the inverted-barometer-corrected sea surface height relative to the geoid. Repeating the correlation/EOF analysis of Peralta-Ferriz and Woodgate (2017) for DOT yields nearly identical results as for the OBP data (correlation between first DOT EOF and PH term $r = 0.48$ for year-round data and $r = 0.82$ for June–July–August [JJA] data; prior OBP values $r = 0.44$ and $r = 0.81$, respectively). This is reassuring, since theoretically the two data sets are closely related. It does, however, pose the question of how the total flow is related to both variables.

In a geostrophically balanced flow,

$$v = -\frac{1}{\rho f}\frac{\partial P}{\partial x}, \tag{1}$$

where v is along-channel velocity; x, cross-channel direction; f, Coriolis parameter; ρ, density of water; and P, in situ pressure, in turn given by:

$$P(z) = \rho_0 g\,\eta + \int_0^z \rho g\, dz' \tag{2}$$

where g is gravitational acceleration; η, sea surface height (i.e., DOT); z, depth; and ρ_0, surface density. Evaluating Equation 2 at $z = H$, (where H is bottom depth) yields a relationship between OBP (defined in equivalent water height, i.e., $P(H)/\rho_0 g$), viz.:

$$\mathrm{OBP} = \mathrm{DOT} + \frac{1}{\rho_0 g}\int_0^H \rho g\, dz', \tag{3}$$

where the second term is the steric contribution.

To obtain the depth-integrated flow, we integrate Equation 1 with respect to z, substituting for P from Equation 2, following standard practice of taking ρ as ρ_o except where differentiated, and assuming for simplicity $\partial\rho/\partial x$ and H are not functions of z or x, resulting in

$$\int_0^H v\, dz = \frac{-gH}{f}\left(\frac{\partial \eta}{\partial x} + \frac{H}{2\,\rho_0}\frac{\partial \rho}{\partial x}\right) \tag{4}$$

Using differentiation of Equation 3 wrt x, we cast Equation 4 in terms of OBP and DOT, that is:

$$\int_0^H v\, dz = \frac{-gH}{f}\frac{\partial}{\partial x}\left(\frac{\mathrm{DOT} + \mathrm{OBP}}{2}\right) \tag{5}$$

Integrating Equation 5 across the strait (i.e., in x) to obtain the entire strait transport, T, and acknowledging we only know changes in DOT and OBP, we find that changes in transport, ΔT, are given by:

$$\Delta T = \frac{-gH}{f}\Delta\left(\frac{\mathrm{DOT} + \mathrm{OBP}}{2}\right) \tag{6}$$

This shows it is the changes of the average of DOT and OBP which drive flow changes. Indeed, repeating Peralta-Ferriz and Woodgate (2017)'s correlation/EOF analysis with this average yields comparable results ($r = 0.5$ year-round, and $r = 0.82$ for JJA).

Furthermore, if we assume as others have (Overland & Roach, 1987) that the cross-strait pressure gradient is comparable to the along-strait, Equation 6 gives a quantitative way of verifying if regression fits we obtain (Section 4) are consistent with theory.

4. Trends in the PH Term, OBP and DOT—Annual and Seasonal

As mentioned above, the updated mooring-based Bering Strait transport estimates (now 1991–2021), show a continuing, significantly increasing trend in northward flow, VVEL, 0.23 ± 0.12 cm/s/year, equivalent to 0.01 ± 0.005 Sv/year, which over the 30-year record, amounts to a significant fraction (~30%) of the long-term annual mean (~1 Sv) (Figure 1a). Updating the analysis of Woodgate (2018), we find this trend is still

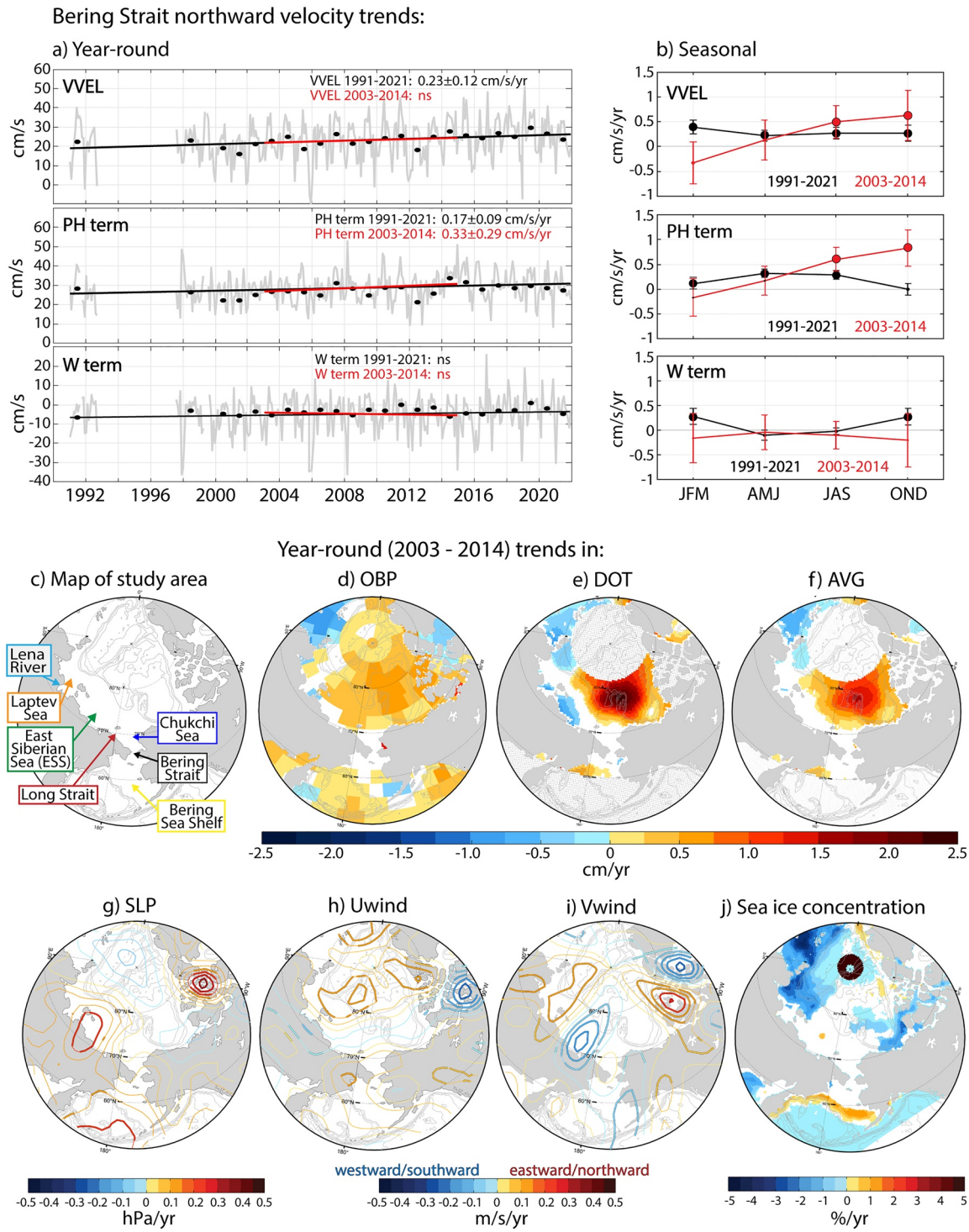

Figure 1. Trends in key Bering Strait parameters. (a) For the entire mooring time-series (1990–2021), monthly (gray) and annual mean (black dots) Bering Strait northward velocity (VVEL), split into pressure-head (PH term) and local wind forced (W term) terms, showing significant trends for the whole time-series and our focus period (2003–2014) (ns indicates not significant). (b) Seasonal trends (with uncertainties, large dot indicating fit significant) for these same parameters. (c) Map with the sub-regions of interest. (d–j) Maps of 2003–2014 year-round trends in Ocean Bottom Pressure (OBP) from the Gravity Recovery and Climate Experiment JPL Mascon Release 6 version 2; Dynamic Ocean Topography (DOT); the average of these (AVG, see Section 3); NCEP Sea Level Pressure (SLP), eastward (Uwind) and westward (Vwind) surface winds; and Special Sensor Microwave Imager sea-ice concentration. White areas in (c)–(f) and (j) indicate no significant trend above the 90% confidence level. Significant trends (above 90% confidence level) in (g)–(i) are highlighted in thick color lines. Black (j) or gray stippled areas around the North Pole and south of 60°N in (e) and (f) indicate locations with no available DOT data. IBCAO bathymetry isobaths (Jakobsson et al., 2008) are shown every 500 m from 500 to 4,500 m (gray lines), with land shaded gray.

19448007, 2023, 24, Downloaded from https://agupubs.onlinelibrary.wiley.com/doi/10.1029/2023GL104697 by Test, Wiley Online Library on [01/01/2024]. See the Terms and Conditions (https://onlinelibrary.wiley.com/terms-and-conditions) on Wiley Online Library for rules of use; OA articles are governed by the applicable Creative Commons License

primarily attributable to an increasing PH term (0.17 ± 0.09 cm/s/year). The subset of this period used for our satellite-based analysis (2003–2014), chosen to match consistent satellite data sets, does not have a significant trend in northward velocity, VVEL (Figure 1) but does still demonstrate the significantly increasing PH term, making it suitable to investigate PH term drivers.

The mechanism of Peralta-Ferriz and Woodgate (2017) predicts that PH term increase should be linked to trends in DOT and OBP—specifically decreasing in the ESS, and/or increasing over the Bering Sea Shelf, probably causally linked with increasing westward winds in the Arctic and/or the Bering Sea. However, of these possible drivers, significant annual mean trends (Figures 1d–1j) are only found in DOT over the ESS. Surprisingly, OBP from GRACE JPL Mascon Release 6, version 2, even increases over the ESS (with this increase being greater in older versions of GRACE, Figure S1 in Supporting Information S1). Westward wind trends are not significant in the annual mean in either relevant region. Neither are Arctic sea-ice trends (which might yield significant trends in ocean surface stress) significant (Figure 1j).

However, recalling Peralta-Ferriz and Woodgate (2017) found different drivers in different seasons, and Woodgate (2018) and Woodgate and Peralta-Ferriz (2021) demonstrated clearer trends in monthly rather than annual mooring data, we examined also trends in monthly values, which we merge here for succinctness into 4 seasons (Figure 2), chosen to combine months with common features. By season (January–March [JFM], April–June [AMJ], etc.), for our 2003–2014 period, VVEL and PH terms now show significant trends in summer (July–September, JAS) and fall (October–December, OND) (Figure 1b), and thus we consider these periods in detail:

Summer (July–September) trends (Figure 2, column 3) support the Peralta-Ferriz and Woodgate (2017) mechanism, with OBP, DOT, and the average of these (AVG)—which theory suggests is the direct driver of the flow (Section 3)—all showing significant decreasing trends in the ESS. We find (Figure 3a, i) AVG in the ESS is significantly and highly ($|r| > 0.8$) correlated with the PH term, and moreover the regression coefficient between these values (Figure 3a, ii), is ∼0.7 ± 0.3 s^{-1} in the ESS, which is in good agreement with the theoretical prediction (C_{AVG}) obtained from Equation 2, viz.:

$$\Delta\text{PHterm} = \frac{\Delta T}{A} = \frac{-gH}{fA}\,\Delta\left(\frac{\text{DOT} + \text{OBP}}{2}\right) = C_{\text{AVG}}\,\Delta\text{AVG} \tag{7}$$

where A is the effective cross-section area of the strait (taken as 85 km × 50 m = 4.25 × 10^6 m^2), yielding (for H of 50 ± 5 m) theoretical values for C_{AVG} of 0.9 ± 0.1 s^{-1}.

We next multiply significant regression values (maps of Figure 3a, i) with significant trends (Figure 2c, column 3, shown also as colored dots on Figure 3a, ii) to obtain a "response" map (Figure 3a, iii), viz. the expected trend in the PH term due to the AVG trend at each grid point. This shows if the trend in the driver is sufficiently large to explain the Bering Strait trend. This response map suggests that the mooring data's summer PH trend (0.6 ± 0.3 cm/s/year, Figure 1b) can be largely explained by ESS AVG change (∼0.4 ± 0.3 cm/s/year when averaged over the ESS, area delimited by the black dots in Figure 3a, i) (Chukchi Sea regions are neglected as being too close to the strait, as compared to the barotropic Rossby radius [∼170 km] or our data footprint [∼300 km] to be independent.).

Overall thus, it appears the observed summer PH trend for our period may be well explained by a drop in AVG in the ESS. In turn, this is likely attributable to an increase in westward winds in this region (Figure 2e, column 3). Creating a "response" map from the ocean surface stress trend and the regression of ocean surface stress with the PH term yields a weaker predicted trend in PH term of ∼0.2 ± 0.15 cm/s/year (Figure 3b, i–iii) (We use surface stress for this regression, rather than wind velocity, as stress is linearly related to the theoretical Ekman transport.). The lesser agreement with this prediction may reflect that our estimate of surface stress neglects sea-ice effects, or simply the noisiness/deficiencies of the winds.

(Note also the *positive* relationship between the PH term and the Beaufort Gyre AVG [increased PH flow correlated with increased Beaufort Gyre AVG], which [rather than being causal] is most likely because the latter is increased by the same wind stress as lowers AVG in the ESS.)

Fall (October–December) trends, in contrast, are not well related to DOT, OBP, or AVG trends (Figures 2a–2f, column 4) in the ESS. The only significant trend in a driver that increases the PH term is an increase in westward winds in the Bering Sea (Figure 2e, column 4). Fall zonal surface stress over both the ESS and the Bering Sea

19448007, 2023, 24, Downloaded from https://agupubs.onlinelibrary.wiley.com/doi/10.1029/2023GL104697 by Test, Wiley Online Library on [01/01/2024]. See the Terms and Conditions (https://onlinelibrary.wiley.com/terms-and-conditions) on Wiley Online Library for rules of use; OA articles are governed by the applicable Creative Commons License

10.1029/2023GL104697

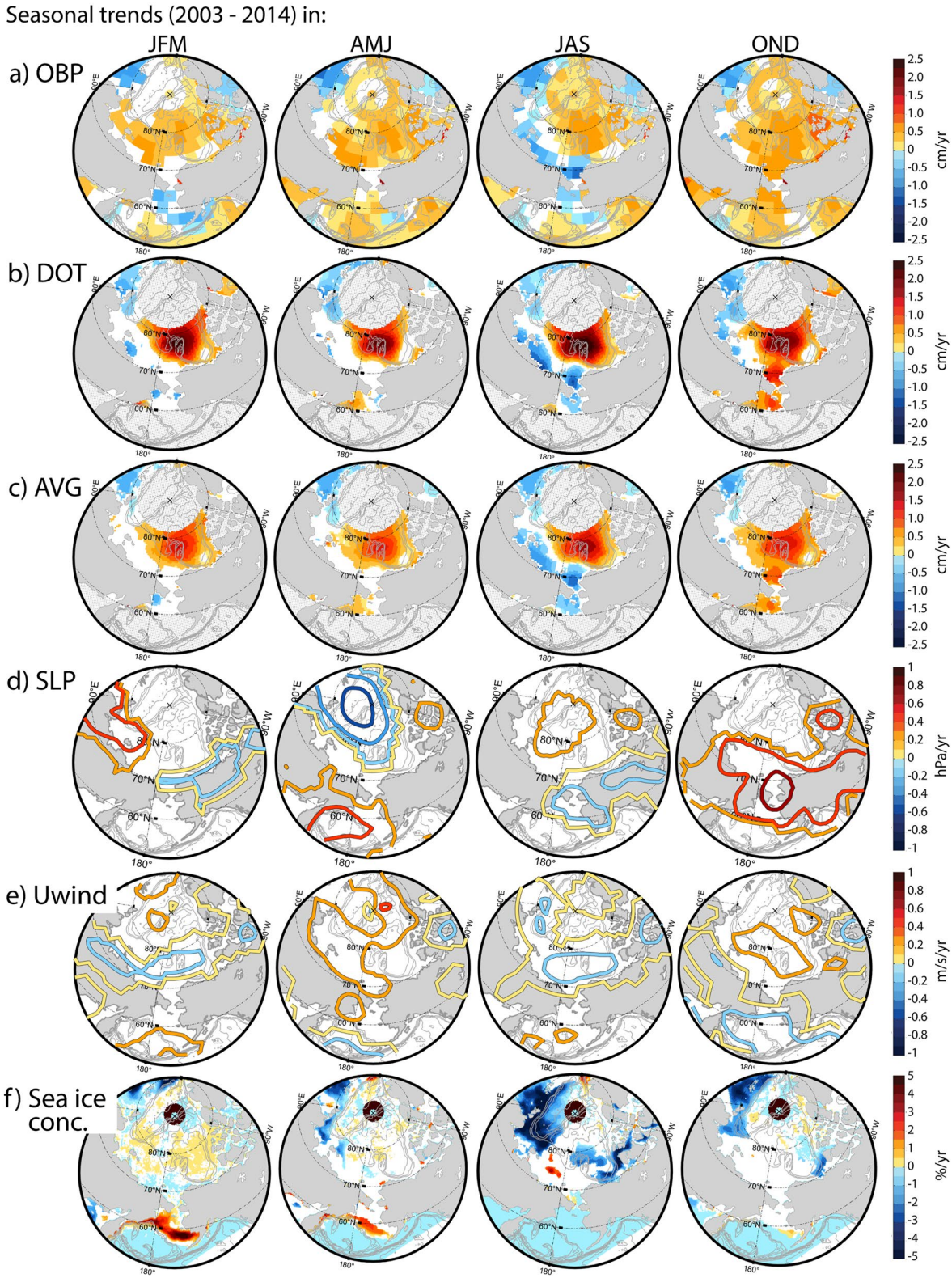

Figure 2. Seasonal trends in key Bering Strait parameters (2003–2014). Row (a–f) variables as per Figures 1d–1j, column indicating season (i.e., column 1 = JFM [January, February, March]; 2 = AMJ [April, May, June]; 3 = JAS [July, August, September]; and 4 = OND [October, November, December]). Trends are plotted only when significant above the 90% confidence level.

19448007, 2023, 24, Downloaded from https://agupubs.onlinelibrary.wiley.com/doi/10.1029/2023GL104697 by Test, Wiley Online Library on [01/01/2024]. See the Terms and Conditions (https://onlinelibrary.wiley.com/terms-and-conditions) on Wiley Online Library for rules of use; OA articles are governed by the applicable Creative Commons License

19448007, 2023, 24, Downloaded from https://agupubs.onlinelibrary.wiley.com/doi/10.1029/2023GL104697 by Test, Wiley Online Library on [01/01/2024]. See the Terms and Conditions (https://onlinelibrary.wiley.com/terms-and-conditions) on Wiley Online Library for rules of use; OA articles are governed by the applicable Creative Commons License

Shelf are well correlated with the PH term (Figure 3c, i), as would be expected from an Ekman relationship, that is,

$$\Delta\text{PHterm (in cm/s)} = \frac{\Delta T}{A} = \frac{100}{\rho f A}\,\Delta\tau_x^{\text{surface}}\,L = C_{\text{WSTR}}\,\Delta\tau_x^{\text{surface}} \tag{8}$$

where τ_x^{surface} is the zonal surface stress and C_{WSTR} is the regression coefficient, which is dependent on L, the east-west distance over which the wind operates. This distance is poorly defined, but C_{WSTR} matches calculated values (Figure 3c, ii, 40–60 [cm/s]/[N/m^2]) for Ls of 100–150 km south of the strait (comparable with the Bering Strait channel width, 85 km at the strait widening to ∼300 km south of the strait) and ∼400 km around the ESS (comparable with length scales of Arctic weather systems [∼100–500 km, Stoll, 2022]). The fall trends in surface stress in the northern Bering Sea (∼10^{-2} N/m^2/year, not shown) acting over a distance of ∼400 km would give ∼1 cm/s/year trend in PH term, comparable to the observed (0.8 ± 0.5 cm/s/year, Figure 1b). Surface stress response maps (Figure 3c, iii) show smaller values (∼0.3 ± 0.2 cm/s/year), but given the substantial errors still may explain a large portion of the observed trend, or, as per the summer results, reflect the generic problem of clear trend estimates from noisy wind data.

Winter (January–March) and Spring (April–June) trends are not significant in the VVEL or PH terms (Figure 1b), and so are not considered further here.

In summary, for our time period (2003–2014), the significant trends in PH term (summer and fall) can likely be explained by increasing westward Arctic winds in summer (decreasing ESS DOT and OBP) and increasing westward Bering Sea winds in fall.

5. Implied Salinization of the East Siberian Sea (ESS)

It is noteworthy that annual (and seasonal) ESS trends in OBP are significantly different to trends in DOT (Figures 1 and 2). If both data sets are reliable, this must indicate a change in density of the ESS waters over our time period, which we quantify to be an annual average densification of order 0.14 kg/m^3/year. MUR SST data (not shown) indicates no significant trend and anyway, at these temperatures (∼−1 to 1°C), temperature has only a small influence on density. Thus, as Armitage et al. (2016), we conclude the data indicate a significant salinization of the region (Figure 3d), 0.17 ± 0.06 psu/year averaged over the ESS (delimited by black dots in Figure 3d), with near coastal areas salinizing by ∼0.4 ± 0.2 psu/year over our 11-year record.

We are unaware of any in situ observations from this period that could test this conclusion. Satellite Surface Salinity products (e.g., Soil Moisture and Ocean Salinity, SMOS, Martínez et al., 2022, and the joint U.S./Argentinian Aquarius/Satélite de Aplicaciones Científicas [SAC]-D mission, Melnichenko et al., 2016) commence only in 2011. Our estimated salinity trends are larger than those of Steele and Ermold (2004), who use World Ocean Data Center data to calculate a trend of 0.07 psu/year for the surface (0–15 m) ESS (1988–2000). However, their value is for a much longer time-period, and *Soil Moisture Active Passive* data from a different (and shorter) period, 2015 to 2020 (Zhuk & Kubryakov, 2021), indicate substantial (∼10 psu) salinity changes in the region, caused by relocation of the fresh Lena River plume in the Laptev Sea, west of the ESS (Figure 1c).

Indeed, displacement of river water by Pacific waters seems the most likely cause of our observed salinization. Other possible causes seem insufficient. Alkire et al. (2017) estimate ESS Precipitation minus Evaporation (P − E) as ∼200 km^3/year. Removing that entire input (assuming ESS salinities of ∼30 psu, area of 1,082 × 10^3 km^2 (Jakobsson et al., 2008), and mixing into a 50 m water column) is equivalent to a ∼0.1 psu salinization, only 5% of our 11-year change of 1.87 psu. To achieve this salinization by brine rejection would require 2 m more ice formation in 2014 than in 2003, an almost 50% increase of the estimated existing seasonal cycle (∼4 m, Arctic Subpolar gyre sTate Estimate [ASTE] data (Nguyen, Pillar, Ocaña, Bigdeli, et al., 2021; Nguyen, Pillar, Ocaña, Smith, & Heimbach, 2021)) and note there are no significant trends in sea-ice concentration in the region (Special Sensor Microwave Imager data, Figure 1j). Even generous estimates of upwelling (e.g., ∼34 psu water from ∼100 m depth) would need to fill ∼10% of the existing depth of the ESS, which seems unlikely. In contrast, increasing the ∼0.1 Sv flow of Pacific water through Long Strait (Woodgate et al., 2005) by only 0.02 Sv per year could yield the observed salinization (assuming Pacific water salinity of 32.5 psu). Furthermore, surface geostrophic velocity (calculated from gradients of DOT, Figure 3e) shows consistent westward flow (∼1–2 cm/s)

10.1029/2023GL104697

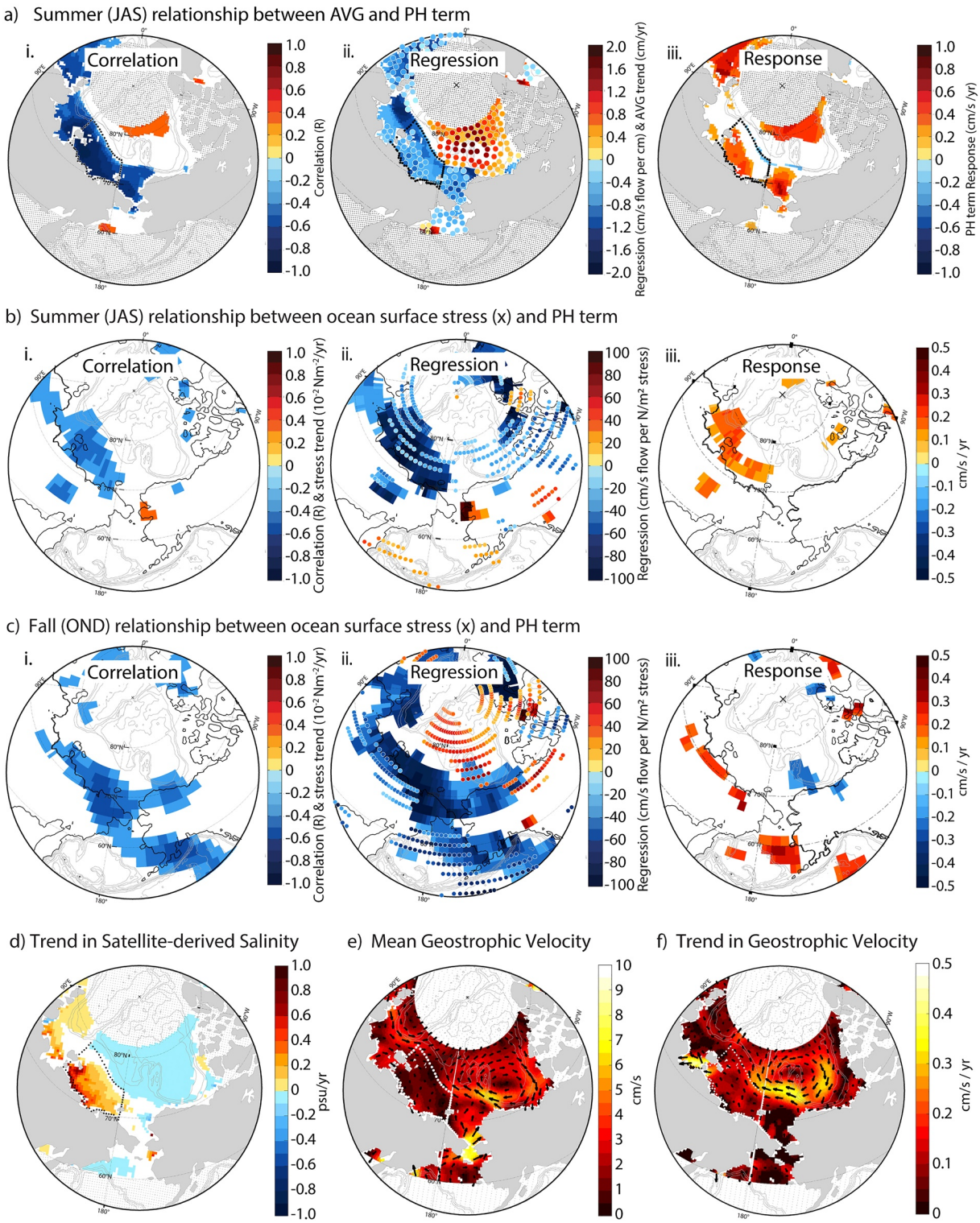

Figure 3. Drivers of Bering Strait and East Siberian Sea (ESS) change. (a) Relationship between summer (July, August, September) AVG and pressure-head (PH) term, showing significant (>95%) coefficients of (i) correlation and (ii) regression (i.e., B of "PH term = A + B × AVG"), and (iii) response (i.e., regression coefficient multiplied by trend, Section 4). Significant trends in AVG (from Figure 2c, column 3) shown also as dots on middle panel. (b) and (c) as per (a) but for surface ocean stress and PH term for (b) summer and (c) fall (October, November, December). Dots in middle panels show significant trends in ocean surface stress (not shown in Figure 2). (d) 2003–2014 annual mean trend in water column average salinity derived from difference of Ocean Bottom Pressure (OBP) and Dynamic Ocean Topography (DOT). (e) 2003–2014 averaged surface geostrophic velocity inferred from DOT (only every tenth vector plotted); and (f) 2003–2014 annual mean trend in surface geostrophic velocity derived from DOT (vectors plotted as in (e)). See Section 5 for discussion.

19448007, 2023, 24, Downloaded from https://agupubs.onlinelibrary.wiley.com/doi/10.1029/2023GL104697 by Test, Wiley Online Library on [01/01/2024]. See the Terms and Conditions (https://onlinelibrary.wiley.com/terms-and-conditions) on Wiley Online Library for rules of use; OA articles are governed by the applicable Creative Commons License

19448007, 2023, 24, Downloaded from https://agupubs.onlinelibrary.wiley.com/doi/10.1029/2023GL104697 by Test, Wiley Online Library on [01/01/2024]. See the Terms and Conditions (https://onlinelibrary.wiley.com/terms-and-conditions) on Wiley Online Library for rules of use; OA articles are governed by the applicable Creative Commons License

of Pacific water into the ESS north of Wrangel Island, with a suitably large increasing trend of 0.024 ± 0.006 Sv (estimated by summing westward flow along a line from the coast up to 74°N, the 100 m isobath, at 180°W and assuming an average depth of 50 m). Thus, it seems that salinization from increased infiltration of Pacific water into the ESS can explain the different OBP and DOT trends.

Three further spin-offs are noteworthy:

a) Increased westward winds in the ESS promote all of these mechanisms—increased Pacific water into the region, upwelling, and sea-ice formation in coastal polynyas.
b) Surface geostrophic velocity maps (Figures 3e and 3f) suggest a much greater proportion of Pacific Water enters the ESS region during this period than is generally realized—the accepted picture being that Pacific Water generally flows eastward along the Alaskan Coast, or enters the Beaufort Gyre (Spall et al., 2018; Timmermans et al., 2014; Timmermans & Toole, 2023). We suggest this increasing westward diversion (yellow region north of Long Strait, Figure 3f) relates to the western displacement of the Arctic's transpolar drift, and this Pacific water infiltration is a hitherto underappreciated corollary of westward displacement of Russian river water entering the Arctic (e.g., Morison et al., 2012; Semiletov et al., 2005; Steele & Boyd, 1998).
c) This mechanism gives a stabilizing feedback. More Pacific water into the ESS densifies the waters, increasing the OBP, and thus slowing the Pacific inflow.

6. Greater Salinization From Older Versions of GRACE

Our calculations with intermediate (i.e., GRACE JPL Mascon Release 6, version 1) and older (i.e., GRACE JPL Mascon Release 5, version 2) versions of GRACE yield intermediate and larger ESS salinization trends (0.27 ± 0.05 psu/year and 0.4 ± 0.06 psu/year, respectively) (see Figure S1 in Supporting Information S1). GRACE JPL Mascon Release 6 and newer use an improved Glacial Isostatic Adjustment model (i.e., ICE-6G_D, Peltier et al., 2018), and Release 6, version 2 (used primarily here) additionally applies updated coefficients to account for the Earth's oblateness and a different processing correction for temporal change in the static gravity field model (Wiese et al., 2018, see release notes). What is remarkable is how much difference this makes—not only to the implied salinization (numbers above), but also to the drivers of the flow. Particularly, the GRACE JPL Mascon versions prior to Release 6, version 2, show either no significant ESS OBP trends in summer (Release 6, version 1), or significant increasing ESS OBP trends in summer (Release 5, version 2, and older versions) (see Figure S2 in Supporting Information S1). These scenarios are either neutral or act to slow down the Bering Strait throughflow.

Overall, this suggests differences between updates of GRACE data are sufficiently large to substantially change forcings of the flow and estimates of salinization.

7. Conclusions and Implications for Modeling of the Bering Strait Throughflow

Using satellite Ocean Bottom Pressure (OBP) and Dynamic Ocean Topography (DOT), we find plausible drivers (westward winds over the East Siberian Sea [ESS] in summer and over the Bering Sea in fall) to explain observed increasing trends in the northward Bering Strait throughflow in those seasons for 2003–2014. Longer satellite data sets are necessary to confirm the drivers of the longer-term increase observed by in situ measurements, and to assess if Arctic or sub-Arctic drivers dominate. For other seasons, we are unable to identify possible drivers, due (we suggest) to noisiness in the data being greater than any trends. Also, even further afield forcing (e.g., de Boer et al., 2018; Nguyen et al., 2020) are not ruled out by our analysis. Our results suggest increased flow of Pacific Water into the ESS significantly salinifies the region (0.17 ± 0.06 psu/year) and the resultant densification in turn diminishes the northward flow through the strait. We find that drivers and salinification are extremely sensitive to the version of GRACE OBP data used.

These results may illuminate why many models fail to correctly simulate the observed Bering Strait flow increase.

a) GRACE JPL Mascon Release 6 version 1 and older versions do not show the necessary decreasing summer trend in OBP. Thus, models assimilating/tuned to these older satellite data sets will be missing a vital forcing of the strait flow. To our knowledge, this includes ASTE (Nguyen, Pillar, Ocaña, Bigdeli, et al., 2021; using JPL Mascon Release 5, version 2), but not Nguyen et al. (2012), which has a more accurate simulation of the Bering Strait flow.

b) Since the Pacific Water is found to enter the ESS driving region, correct simulation of the salinity of the Bering Strait throughflow appears essential to maintain the correct forcing. We note that Nguyen et al. (2012), which reproduced the Bering Strait flow well, also well-matched Bering Strait salinities, whereas ASTE (Nguyen, Pillar, Ocaña, Bigdeli, et al., 2021), which does not obtain the increasing flow trend, has Bering Strait salinities (Nguyen, Pillar, Ocaña, Smith, & Heimbach, 2021) ∼0.6 psu higher than observations. By Equation 7, assuming DOT remains constant, that salinity change in the ESS would reduce the flow by ∼1.4 cm/s, equivalent to ∼7 years of the long-term observational trend.

c) Since wind-driven lowering of OBP and DOT in the ESS is a dominant mechanism, model results may also be sensitive to inadequacies in wind-water coupling in a region with seasonal sea ice.

These sensitivities suggest a rather fine balance of forces determining the trend in the Bering Strait throughflow. While it implies that observed freshening of the throughflow (0.03 psu/year in winter, Woodgate & Peralta-Ferriz, 2021), attributed to increased runoff from the Alaskan coast, may also have a modest dynamic and accelerating effect on the throughflow, that effect is only (currently) small (PH term increase ∼0.07 cm/s/year), order 10% of the observed long-term trend. However, sensitivities to versions of satellite data products leaves us currently unable to reliably estimate changes in the flow from remote data alone, leaving in situ moorings as the only reliable way of quantifying change in the Pacific inflow to the Arctic.

Data Availability Statement

Our data sources are: Bering Strait mooring data from the National Centers for Environmental Information (https://www.ncei.noaa.gov/), with data and products (e.g., monthly and annual means) from the Bering Strait project website, http://psc.apl.washington.edu/BeringStrait.html (Woodgate, 2018; Woodgate et al., 2015; Woodgate & Peralta-Ferriz, 2021); Arctic DOT and geostrophic currents from University College London's Center for Polar Observation and Modeling, http://www.cpom.ucl.ac.uk/dynamic_topography/ (Armitage et al., 2016); GRACE JPL Mascon Release 6, version 2, as well as Release 6 version 1 and Release 5 version 2, OBP data from NASA's PO.DAAC, https://podaac.jpl.nasa.gov (Watkins et al., 2015; Wiese et al., 2018); NCEP-NCAR Reanalysis 1 atmospheric data from NOAA PSL, https://psl.noaa.gov/data/gridded/data.ncep.reanalysis.html (Kalnay et al., 1996); NOAA/NSIDC Passive Microwave Sea Ice Concentrations from the National Snow and Ice Data Center (Meier et al., 2017; Peng et al., 2013); MUR SST from NASA'S PO.DAAC (Chin et al., 2017; JPL MUR MEaSUREs Project, 2015); and bathymetry data from the International Bathymetric Chart of the Arctic Ocean (IBCAO) version 2.23, https://www.gebco.net/about_us/committees_and_groups/scrum/ibcao/ibcao_v2_23.html (Jakobsson et al., 2008).

Acknowledgments
We thank An Nguyen and David Wiese for informative discussions, and Seth Danielson and an anonymous reviewer for their helpful comments. This work was supported by NSF AON Grants PLR-1758565 and PLR-2153942, and NASA Grant 80NSSC20K0763.

References

Alkire, M. B., Morison, J., Schweiger, A., Zhang, J., Steele, M., Peralta-Ferriz, C., & Dickinson, S. (2017). A meteoric water budget for the Arctic Ocean. *Journal of Geophysical Research: Oceans*, *122*(12), 10020–10041. https://doi.org/10.1002/2017JC012807

Armitage, T. W. K., Bacon, S., Ridout, A. L., Thomas, S. F., Aksenov, Y., & Wingham, D. J. (2016). Arctic sea surface height variability and change from satellite radar altimetry and GRACE, 2003–2014. *Journal of Geophysical Research: Oceans*, *121*(6), 4303–4322. https://doi.org/10.1002/2015JC011579

Chin, T. M., Vazquez-Cuervo, J., & Armstrong, E. M. (2017). A multi-scale high-resolution analysis of global sea surface temperature. *Remote Sensing of Environment*, *200*, 154–169. https://doi.org/10.1016/j.rse.2017.07.029

Coachman, L. K., & Aagaard, K. (1966). On the water exchange through Bering Strait. *Limnology & Oceanography*, *11*(1), 44–59. https://doi.org/10.4319/lo.1966.11.1.0044

Danielson, S. L., Weingartner, T. J., Hedstrom, K. S., Aagaard, K., Woodgate, R., Curchitser, E., & Stabeno, P. J. (2014). Coupled wind-forced controls of the Bering–Chukchi shelf circulation and the Bering Strait throughflow: Ekman transport, continental shelf waves, and variations of the Pacific–Arctic sea surface height gradient. *Progress in Oceanography*, *125*, 40–61. https://doi.org/10.1016/j.pocean.2014.04.006

de Boer, A. M., Gavilan Pascual-Ahuir, E., Stevens, D. P., Chafik, L., Hutchinson, D. K., Zhang, Q., et al. (2018). Interconnectivity between volume transports through Arctic straits. *Journal of Geophysical Research: Oceans*, *123*(12), 8714–8729. https://doi.org/10.1029/2018JC014320

de Boer, A. M., & Nof, D. (2004a). The Bering Strait is grip on the Northern Hemisphere climate. *Deep Sea Research Part I: Oceanographic Research Papers*, *51*(10), 1347–1366. https://doi.org/10.1016/j.dsr.2004.05.003

de Boer, A. M., & Nof, D. (2004b). The exhaust valve of the North Atlantic. *Journal of Climate*, *17*(3), 417–422. https://doi.org/10.1175/1520-0442(2004)017<0417:TEVOTN>2.0.CO;2

Jahn, A., & Laiho, R. (2020). Forced changes in the Arctic freshwater budget emerge in the early 21st century. *Geophysical Research Letters*, *47*(15), e2020GL088854. https://doi.org/10.1029/2020GL088854

Jakobsson, M., Macnab, R., Mayer, L. A., Anderson, R., Edwards, M., Hatzky, J., et al. (2008). An improved bathymetric portrayal of the Arctic Ocean: Implications for ocean modeling and geological, geophysical and oceanographic analyses. *Geophysical Research Letters*, *35*(7), L07602. https://doi.org/10.1029/2008gl033520

JPL MUR MEaSUREs Project. (2015). GHRSST Level 4 MUR Global Foundation sea surface temperature analysis Ver. 4.1 [Dataset]. PO.DAAC. https://doi.org/10.5067/GHGMR-4FJ04

19448007, 2023, 24, Downloaded from https://agupubs.onlinelibrary.wiley.com/doi/10.1029/2023GL104697 by Test, Wiley Online Library on [01/01/2024]. See the Terms and Conditions (https://onlinelibrary.wiley.com/terms-and-conditions) on Wiley Online Library for rules of use; OA articles are governed by the applicable Creative Commons License

Kalnay, E., Kanamitsu, M., Kistler, R., Collins, W., Deaven, D., Gandin, L., et al. (1996). The NCEP/NCAR 40-year reanalysis project [Dataset]. Bulletin America Meteorology Social, *77*(3), 437–472. https://doi.org/10.1175/1520-0477(1996)077<0437:TNYRP>2.0.CO;2

Martínez, J., Gabarró, C., Turiel, A., González-Gambau, V., Umbert, M., Hoareau, N., et al. (2022). Improved BEC SMOS Arctic sea surface salinity product v3.1 [Dataset]. Earth System Science Data, *14*(1), 307–323. https://doi.org/10.5194/essd-14-307-2022

Meier, W. N., Fetterer, F., Savoie, M., Mallory, S., Duerr, R., & Stroeve, J. (2017). NOAA/NSIDC climate data record of passive microwave sea ice concentration Version 3 [Dataset]. NSIDC: National Snow and Ice Data Center. https://doi.org/10.7265/N59P2ZTG

Melnichenko, O., Hacker, P., Maximenko, N., Lagerloef, G., & Potemra, J. (2016). Optimum interpolation analysis of Aquarius sea surface salinity. *Journal of Geophysical Research: Oceans*, *121*(1), 602–616. https://doi.org/10.1002/2015JC011343

Morison, J., Kwok, R., Peralta-Ferriz, C., Alkire, M., Rigor, I., Andersen, R., & Steele, M. (2012). Changing Arctic Ocean freshwater pathways. *Nature*, *481*(7379), 66–70. PMID: 22222749. https://doi.org/10.1038/nature10705

Nguyen, A. T., Kwok, R., & Menemenlis, D. (2012). Source and pathway of the Western Arctic upper halocline in a data-constrained coupled ocean and sea ice model. *Journal of Physical Oceanography*, *42*(5), 802–823. https://doi.org/10.1175/jpo-d-11-040.1

Nguyen, A. T., Pillar, H., Ocaña, V., Bigdeli, A., Smith, T. A., & Heimbach, P. (2021). The Arctic Subpolar gyre sTate Estimate: Description and assessment of a data-constrained, dynamically consistent ocean-sea ice estimate for 2002–2017. *Journal of Advances in Modeling Earth Systems*, *13*(5), e2020MS002398. https://doi.org/10.1029/2020MS002398

Nguyen, A. T., Pillar, H., Ocaña, V., Smith, T., & Heimbach, P. (2021). Arctic Subpolar gyre sTate Estimate Release 1 (ASTE_R1) data 2002-2017, monthly averages and snapshots [Dataset]. Arctic Data Center. https://doi.org/10.18739/A2CV4BS5K

Nguyen, A. T., Woodgate, R. A., & Heimbach, P. (2020). Elucidating large-scale atmospheric controls on Bering Strait throughflow variability using a data-constrained ocean model and its adjoint. *Journal of Geophysical Research: Ocean*, *125*(9), e2020JC016213. https://doi.org/10.1029/2020JC016213

Overland, J. E., & Roach, A. T. (1987). Northward flow in the Bering and Chukchi seas. *Journal of Geophysical Research*, *92*(C7), 7097–7105. https://doi.org/10.1029/JC092iC07p07097

Peltier, W. R., Argus, D. F., & Drummond, R. (2018). Comment on "An assessment of the ICE-6G_C (VM5a) glacial isostatic adjustment model" by Purcell et al. *Journal of Geophysical Research: Solid Earth*, *123*, 2019–2028. https://doi.org/10.1002/2016JB013844

Peng, G., Meier, W. N., Scott, D., & Savoie, M. (2013). A long-term and reproducible passive microwave sea ice concentration data record for climate studies and monitoring. *Earth System Science Data*, *5*(2), 311–318. https://doi.org/10.5194/essd-5-311-2013

Peralta-Ferriz, C., & Woodgate, R. A. (2017). The dominant role of the East Siberian Sea in driving the oceanic flow through the Bering Strait—Conclusions from GRACE ocean mass satellite data and *in situ* Mooring observations between 2002 and 2016. *Geophysical Research Letters*, *44*(22), 11–472. https://doi.org/10.1002/2017gl075179

Semiletov, I., Dudarev, O., Luchin, V., Charkin, A., Shin, K.-H., & Tanaka, N. (2005). The East Siberian Sea as a transition zone between Pacific-derived waters and Arctic shelf waters. *Geophysical Research Letters*, *32*(10), L10614. https://doi.org/10.1029/2005GL022490

Spall, M., Pickart, R., Li, M., Itoh, M., Lin, P., Kikuchi, T., & Qi, Y. (2018). Transport of Pacific water into the Canada Basin and the formation of the Chukchi Slope Current. *Journal of Geophysical Research: Oceans*, *123*(10), 7453–7471. https://doi.org/10.1029/2018JC013825

Steele, M., & Boyd, T. (1998). Retreat of the cold halocline layer in the Arctic Ocean. *Journal of Geophysical Research*, *103*(C5), 10419–10435. https://doi.org/10.1029/98JC00580

Steele, M., & Ermold, W. (2004). Salinity trends on the Siberian shelves. *Geophysical Research Letters*, *31*(24), L24308. https://doi.org/10.1029/2004GL021302

Stigebrandt, A. (1984). The North Pacific: A global-scale estuary. *Journal of Physical Oceanography*, *14*, 464–470. https://doi.org/10.1175/1520-0485(1984)014⟨0464:TNPAGS⟩2.0.CO;2

Stoll, P. J. (2022). A global climatology of polar lows investigated for local differences and wind-shear environments. *Weather Climate Dynamics*, *3*(2), 483–504. https://doi.org/10.5194/wcd-3-483-2022

Tapley, B. D., Bettadpur, S., Watkins, M., & Reigber, C. (2004). The gravity recovery and climate experiment: Mission overview and early results. *Geophysical Research Letters*, *31*(9), L09607. https://doi.org/10.1029/2004GL019920

Tapley, B. D., Watkins, M. M., Flechtner, F., Reigber, C., Bettadpur, S., Rodell, M., et al. (2019). Contributions of GRACE to understanding climate change. *Nature Climate Change*, *9*(5), 358–369. https://doi.org/10.1038/s41558-019-0456-2

Timmermans, M.-L., Proshutinsky, A., Golubeva, E., Jackson, J. M., Krishfield, R., McCall, M., et al. (2014). Mechanisms of Pacific Summer Water variability in the Arctic's Central Canada Basin. *Journal of Geophysical Research: Oceans*, *119*(11), 7523–7548. https://doi.org/10.1002/2014JC010273

Timmermans, M.-L., & Toole, J. M. (2023). The Arctic Ocean's Beaufort Gyre. *Annual Review of Marine Science*, *15*(1), 223–248. https://doi.org/10.1146/annurev-marine-032122-012034

Toulany, B., & Garrett, C. (1984). Geostrophic control of fluctuating barotropic flow through straits. *Journal of Physical Oceanography*, *14*(4), 649–655. https://doi.org/10.1175/1520-0485(1984)014<0649:GCOFBF>2.0.CO;2

Watkins, M. M., Wiese, D. N., Yuan, D. N., Boening, C., & Landerer, F. W. (2015). Improved methods for observing Earth's time variable mass distribution with GRACE using spherical cap mascons: Improved gravity observations from GRACE. *Journal of Geophysical Research: Solid Earth*, *120*, 4. https://doi.org/10.1002/2014JB011547

Wiese, D. N., Landerer, F. W., & Watkins, M. M. (2016). Quantifying and reducing leakage errors in the JPL RL05M GRACE mascon solution. *Water Resources Research*, *52*(9), 7490–7502. https://doi.org/10.1002/2016WR019344

Wiese, D. N., Yuan, D.-N., Boening, C., Landerer, F. W., & Watkins, M. M. (2018). JPL GRACE Mascon Ocean, ice, and hydrology equivalent water height RL06 CRI filtered Version 1. Ver. 1.0 [Dataset]. PO.DAAC. https://doi.org/10.5067/TEMSC-3MJC6

Woodgate, R. A. (2018). Increases in the Pacific inflow to the Arctic from 1990 to 2015, and insights into seasonal trends and driving mechanisms from year-round Bering Strait mooring data. *Progress in Oceanography*, *160*, 124–154. https://doi.org/10.1016/j.pocean.2017.12.007

Woodgate, R. A., Aagaard, K., & Weingartner, T. J. (2005). A year in the physical oceanography of the Chukchi Sea: Moored measurements from autumn 1990–1991. *Deep Sea Research Part II: Topical Studies in Oceanography*, *52*(24–26), 3116–3149. https://doi.org/10.1016/j.dsr2.2005.10.016

Woodgate, R. A., & Peralta-Ferriz, C. (2021). Warming and freshening of the Pacific inflow to the Arctic from 1990–2019 implying dramatic shoaling in Pacific Winter Water ventilation of the Arctic water column. *Geophysical Research Letters*, *48*(9), e2021GL092528. https://doi.org/10.1029/2021GL092528

Woodgate, R. A., Stafford, K. M., & Prahl, F. G. (2015). A synthesis of year-round interdisciplinary mooring measurements in the Bering Strait (1990–2014) and the RUSALCA years (2004–2011). *Oceanography*, *28*(3), 46–67. https://doi.org/10.5670/oceanog.2015.57

Zhuk, V. R., & Kubryakov, A. A. (2021). Interannual variability of the Lena River Plume propagation in 1993–2020 during the ice-free period on the base of satellite salinity, temperature, and altimetry measurements. *Remote Sensing*, *13*(21), 4252. https://doi.org/10.3390/rs13214252

19448007, 2023, 24, Downloaded from https://agupubs.onlinelibrary.wiley.com/doi/10.1029/2023GL104697 by Test, Wiley Online Library on [01/01/2024]. See the Terms and Conditions (https://onlinelibrary.wiley.com/terms-and-conditions) on Wiley Online Library for rules of use; OA articles are governed by the applicable Creative Commons License